




Crystal structure of halofuginone hydrobromide, C₁₆H₁₈BrClN₃O₃BrJames A. Kaduk ^{1,2,a)} Stacy Gates-Rector ³ and Thomas N. Blanton ³¹Illinois Institute of Technology, 3101 S. Dearborn St., Chicago, IL 60616, USA²North Central College, 131 S. Loomis St., Naperville, IL 60540, USA³ICDD, 12 Campus Blvd., Newtown Square, PA 19073-3273, USA

(Received 28 June 2022; accepted 23 September 2022)

The crystal structure of one form of halofuginone hydrobromide has been solved and refined using synchrotron X-ray powder diffraction data, and optimized using density functional theory techniques. Halofuginone hydrobromide crystallizes in space group $P2_1$ (#4) with $a = 8.87398(13)$, $b = 14.25711(20)$, $c = 15.0153(3)$ Å, $\beta = 91.6867(15)^\circ$, $V = 1898.87(4)$ Å³, and $Z = 4$. The crystal structure consists of alternating layers (parallel to the ab -plane) of planar and nonplanar portions of the cations. N–H⋯Br and O–H⋯Br hydrogen bonds link the protonated piperidine rings and bromide anions into a two-dimensional network parallel to the ab -plane. The powder pattern has been submitted to ICDD for inclusion in the Powder Diffraction File™ (PDF®). © The Author(s), 2022. Published by Cambridge University Press on behalf of International Centre for Diffraction Data. This is an Open Access article, distributed under the terms of the Creative Commons Attribution licence (<http://creativecommons.org/licenses/by/4.0/>), which permits unrestricted re-use, distribution and reproduction, provided the original article is properly cited. [doi:10.1017/S088571562200046X]

Key words: halofuginone, Stenorol, powder diffraction, Rietveld refinement, density functional theory

I. INTRODUCTION

Halofuginone hydrobromide (sold under the brand names Stenorol and Tempostatin) is a semisynthetic quinazolinone alkaloid anticoccidial derived from the plant *Dichroa febrifuga*, with antifibrotic and potential antineoplastic activities. It has been registered as an anticoccidial feed additive for broiler hens and turkeys (EMEA, 2000). Halofuginone specifically inhibits collagen type I gene expression and matrix metalloproteinase 2 (MMP-2) gene expression, which may result in the suppression of angiogenesis, tumor stromal cell development, and tumor cell growth. These effects appear to be due to halofuginone-mediated inhibition of the collagen type I and MMP-2 promoters. Collagen type I and MMP-2 play important roles in fibro-proliferative diseases (National Cancer Institute, https://ncithesaurus.nci.nih.gov/ncitbrowser/ConceptReport.jsp?dictionary=NCI_Thesaurus&version=21.08e&code=C2656&ns=ncit). Halofuginone hydrobromide was used for the treatment of Duchenne muscular dystrophy, but has been withdrawn. Halofuginone is a low molecular weight quinazolinone alkaloid, and a potent inhibitor of collagen alpha1(I) and matrix metalloproteinase 2 (MMP-2) gene expression. Halofuginone also effectively suppresses tumor progression and metastasis in mice. Collgard Biopharmaceuticals is developing halofuginone for the treatment of scleroderma and received orphan drug designation from the U.S. Food and Drug Administration in March 2000 (Drugbank, <https://go.drugbank.com/salts/DBSALT000462>). The systematic name (CAS Registry Number 64924-67-0) is 7-bromo-6-chloro-3-[3-[(2S,3R)-3-hydroxypiperidin-2-yl]-2-

oxopropyl]quinazolin-4-one hydrobromide. A two-dimensional molecular diagram is shown in Figure 1. We are unaware of any published X-ray powder diffraction data on this compound.

This work was carried out as part of a project (Kaduk *et al.*, 2014) to determine the crystal structures of large-volume commercial pharmaceuticals, and include high-quality powder diffraction data for them in the Powder Diffraction File (Gates-Rector and Blanton, 2019).

II. EXPERIMENTAL

Halofuginone hydrobromide is a commercial reagent, purchased from TargetMol (Lot #117287), and was used as-received. The white powder was packed into a 1.5 mm diameter Kapton capillary and rotated during the measurement at ~50 Hz. The powder pattern was measured at 295 K at beamline 11-BM (Antao *et al.*, 2008; Lee *et al.*, 2008; Wang *et al.*, 2008) of the Advanced Photon Source at Argonne National Laboratory using a wavelength of 0.458963(2) Å from 0.5 to 50° 2θ with a step size of 0.0009984375 and a counting time of 0.1 s step⁻¹. The high-resolution powder diffraction data were collected using twelve silicon crystal analyzers that allow for high angular resolution, high precision, and accurate peak positions. A mixture of silicon (NIST SRM 640c) and alumina (NIST SRM 676a) standards (ratio Al₂O₃: Si = 2:1 by weight) was used to calibrate the instrument and refine the monochromatic wavelength used in the experiment.

The pattern was difficult to index. The cell used here (primitive monoclinic with $a = 8.9459$, $b = 14.2647$, $c = 15.0265$ Å, $\beta = 91.193^\circ$, $V = 1917.3$ Å³) was obtained by DICVOL14 (Louër and Boulton, 2014) using 23 peaks with $I_{rel} > 1$, and permitting up to 5 unindexed lines. The unit cell

^{a)} Author to whom correspondence should be addressed. Electronic mail: kaduk@polycrystallography.com

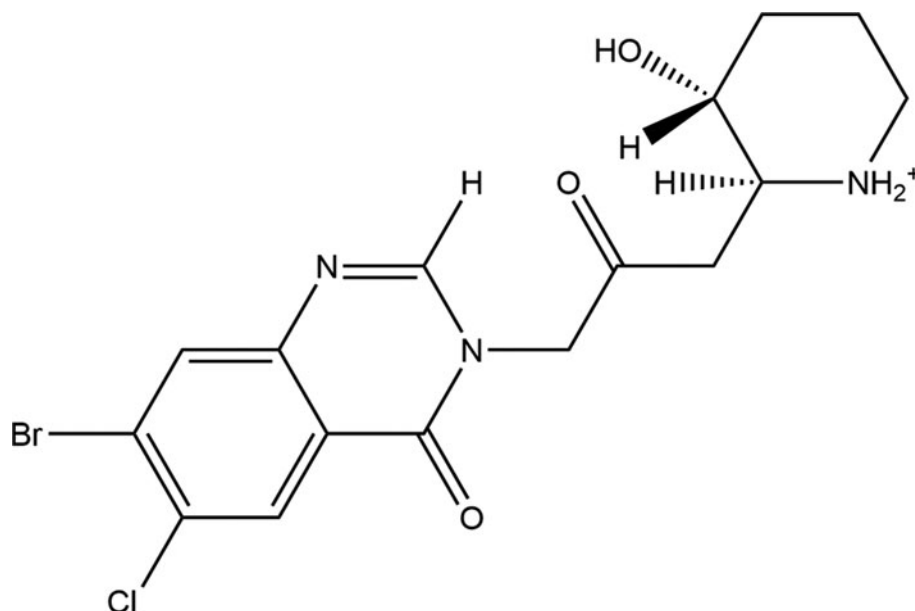


Figure 1. The 2D molecular structure of the halofuginone cation.

volume (assuming $18 \text{ \AA}^3/\text{heavy atom}$, because of the large Br atoms) corresponds to $Z=4$. The space group suggested by EXPO2014 (Altomare *et al.*, 2013) was $P2_1$, which was confirmed by successful solution and refinement of the structure. This is, thus, a larger-than-expected structure (more variables), as there are two independent cations and two bromide anions in the asymmetric unit. A reduced cell search in the Cambridge Structural Database (Groom *et al.*, 2016) with the chemistry H, C, Br, Cl, N, and O only yielded no hits.

This unit cell does not index all of the observed peaks. Attempts to index the remaining peaks on a single unit cell failed, suggesting that at least two impurity phases are present. The European Agency for the Evaluation of Medicinal Products report (2000) indicates that *trans*-halofuginone is the active ingredient, and that the *cis*-isomer is present as an impurity. It may, thus, not be unexpected that the pattern was difficult to index.

A halofuginone molecule was downloaded from PubChem (Kim *et al.*, 2019) as Conformer3D_CID_400772.sdf. It was converted to a*.mol2 file using Mercury (Macrae *et al.*, 2020). The structure was solved by Monte Carlo simulated annealing as implemented in EXPO2014 (Altomare *et al.*, 2013). It was easy to conclude that N6 and N47 in the saturated rings were protonated, so H85 and H86 were added to these nitrogen atoms using Materials Studio (Dassault, 2021).

Rietveld refinement was carried out using GSAS-II (Toby and Von Dreele, 2013). Only the $1.5\text{--}25.0^\circ$ portion of the pattern was included in the refinement ($d_{\text{min}} = 1.060 \text{ \AA}$). The presence of multiple Br atoms means that, even using synchrotron radiation, the sample is absorbing. A value $\mu R = 0.54$ (calculated using a tool on the 11-BM Web site, <https://11bm.xray.aps.anl.gov/absorb/absorb.php>) was included in the refinement. The y -coordinate of Br1 was fixed to define the origin. All non-H bond distances and angles (plus the planes of the fused ring systems) were subjected to restraints, based on a Mercury/Mogul Geometry Check (Bruno *et al.*, 2004; Sykes *et al.*, 2011). The Mogul average and standard deviation for each quantity were used as the restraint parameters. The

restraints contributed 3.0% to the final χ^2 . The hydrogen atoms were included in calculated positions, which were recalculated during the refinement using Materials Studio (Dassault, 2021). The U_{iso} of the heavy atoms were grouped by chemical similarity. The U_{iso} for the H atoms were fixed at $1.2 \times$ the U_{iso} of the heavy atoms to which they are attached. The peak profiles were described using a uniaxial microstrain model, with [001] as the unique axis, chosen on the basis of the BFDH morphology discussed below. A fourth-order spherical harmonic preferred orientation model was included in the refinement. The texture index was 1.020(1). The background was modeled using a 6-term shifted Chebyshev polynomial, and a peak at $7.03^\circ 2\theta$ to model the scattering from the Kapton capillary and any amorphous component.

The final refinement (which was begun from the VASP-optimized structure) of 181 variables using 23 538 observations and 128 restraints yielded the residuals $R_{\text{wp}} = 0.1134$ and $\text{GOF} = 2.65$. The largest peak (1.18 \AA from C53) and hole (1.20 \AA from H75) in the difference Fourier map were $0.64(14)$ and $-0.51(14) e\text{\AA}^{-3}$, respectively. The largest intensity differences in the difference plot occur at the impurity peaks, as observable in Figure 2.

The crystal structure was optimized using VASP (Kresse and Furthmüller, 1996) (fixed experimental unit cell) through the MedeA graphical interface (Materials Design, 2016). The calculation was carried out on 16 2.4 GHz processors (each with 4 GB RAM) of a 64-processor HP Proliant DL580 Generation 7 Linux cluster at North Central College. The calculation used the GGA-PBE functional, a plane wave cutoff energy of 400.0 eV, and a k -point spacing of 0.5 \AA^{-1} leading to a $2 \times 1 \times 1$ mesh, and took ~ 30 h. A single-point density functional calculation (fixed experimental cell) and population analysis were carried out using CRYSTAL17 (Dovesi *et al.*, 2018). The basis sets for the H, C, N, and O atoms in the calculation were those of Gatti *et al.* (1994), and those for Br and Cl were those of Peintinger *et al.* (2013). The calculations were run on a 3.5 GHz PC using 8 k -points and the B3LYP functional, and took ~ 5.7 h.

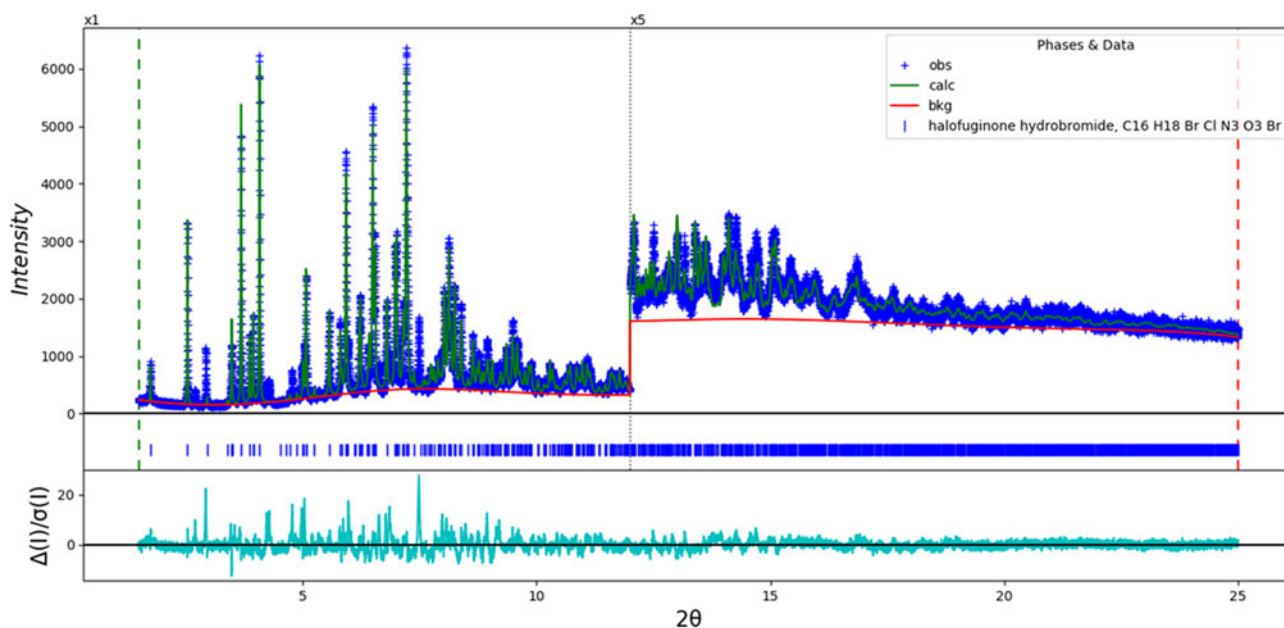


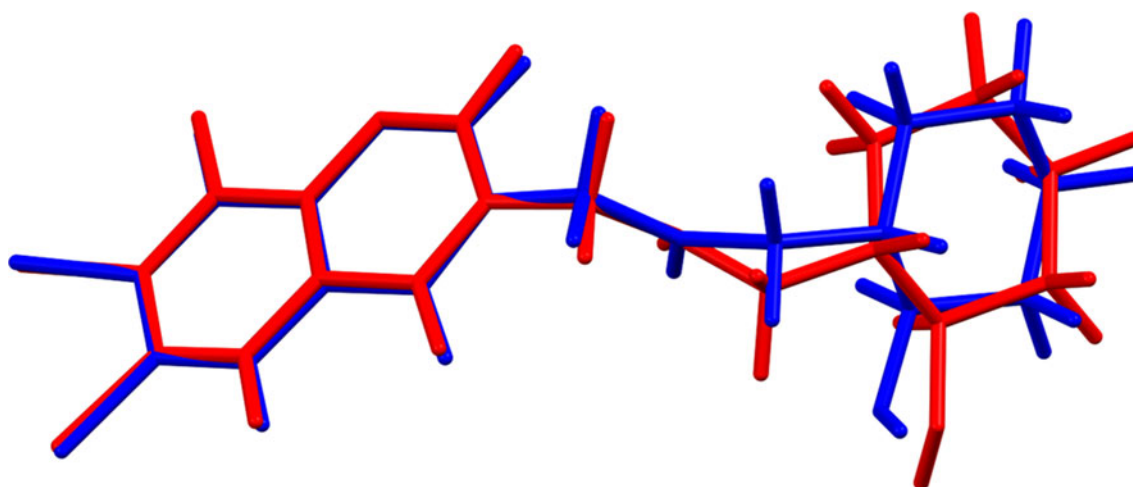
Figure 2. The Rietveld plot for the refinement of halofuginone hydrobromide. The blue crosses represent the observed data points, and the green line is the calculated pattern. The cyan curve is the normalized error plot. The vertical scale of the observed and calculated plots has been multiplied by a factor of 5 \times for $2\theta > 12.0^\circ$. The row of blue tick marks indicates the calculated reflection positions.

III. RESULTS AND DISCUSSION

This form of halofuginone hydrobromide crystallizes in space group $P2_1$ with $Z=4$. Neither the 'Find Symmetry' module of Materials Studio nor the ADDSYM function of PLATON (Spek, 2009) revealed any additional symmetry in the refined or optimized structures. The root-mean-square (rms) Cartesian displacements between the Rietveld-refined and DFT-optimized structures of halofuginone hydrobromide are 0.338 Å for cation 1 (the lower atom numbers) and 0.500 Å for cation 2 (higher atom numbers) (Figures 3 and 4). The largest differences in each cation are at the hydroxyl groups O3 and O44 on the piperidine rings. The agreement for cation 1 is at the high end for correct powder structures (van de

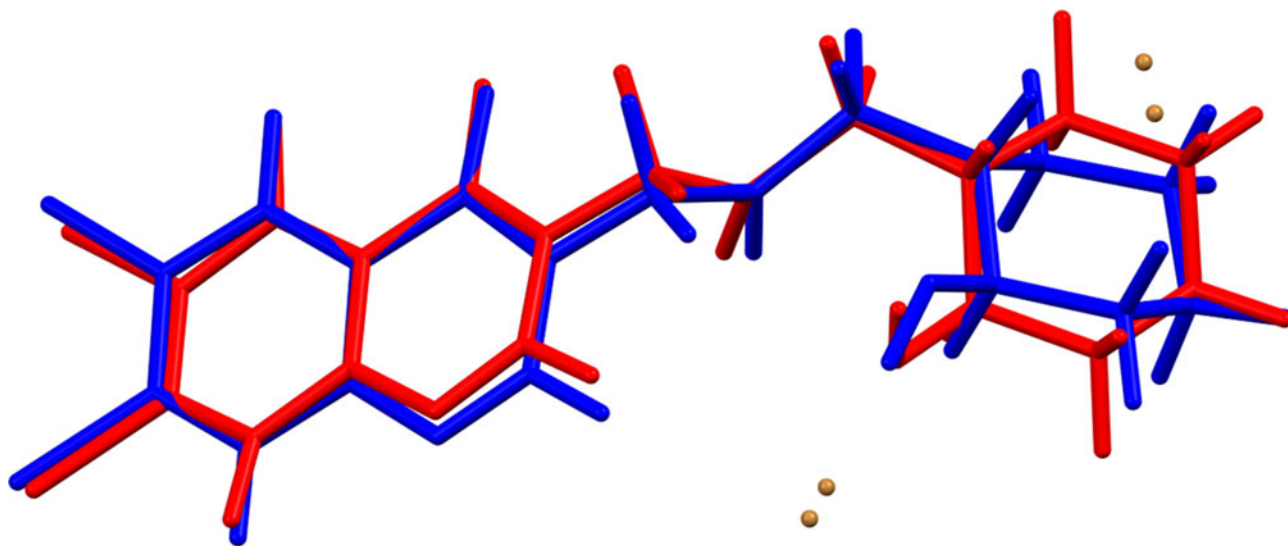
Streek and Neumann, 2014), while that for cation 2 is outside the normal range. The asymmetric unit (with atom numbering) is illustrated in Figure 5. The displacement coefficients of the atoms in the piperidine ring of cation 2 are larger than those of the other atoms, suggesting that there is something unusual about this ring. The chirality of both atoms in both cations in both the refined and optimized structures, is the same and correct (*S* for C9 and C50 and *R* for C10 and C51), showing that no inversion occurred during refinement or optimization.

The two independent cations in the refined structure have different conformations (Figure 6). The rms Cartesian displacement is 1.773 Å. When the 'inversion' option in Mercury Calculate Molecule Overlay is invoked, the



Molecule 1; rmsd = 0.338; max = 0.821 at O3

Figure 3. Comparison of the Rietveld-refined (red) and VASP-optimized (blue) structures of cation 1 in halofuginone hydrobromide. The rms Cartesian displacement is 0.338 Å. Image generated using Mercury (Macrae *et al.*, 2020).



Molecule 2; rmsd = 0.500; max = 1.006 at O44

Figure 4. Comparison of the Rietveld-refined (red) and VASP-optimized (blue) structures of cation 2 in halofuginone hydrobromide. The rms Cartesian displacement is 0.500 Å. Image generated using Mercury (Macrae *et al.*, 2020).

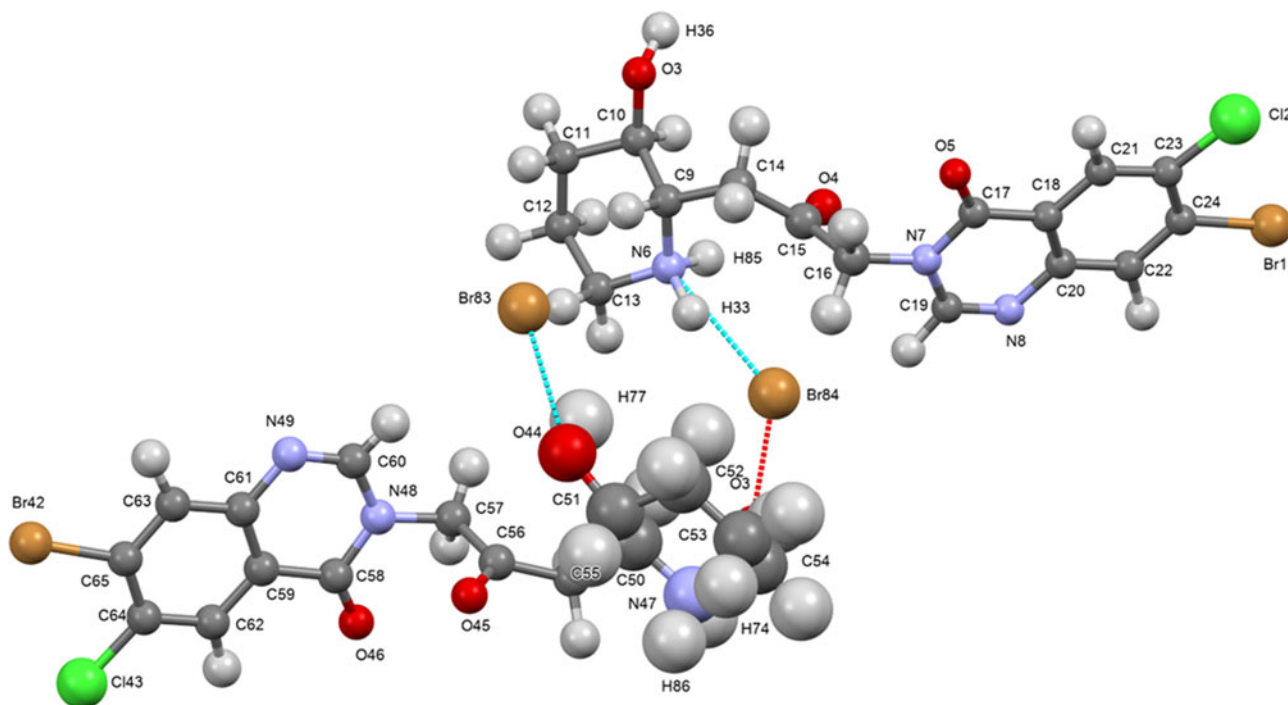


Figure 5. The asymmetric unit of halofuginone hydrobromide, with the atom numbering. The atoms are represented by 50% probability spheroids. Cation 1 has the smaller atom numbers, and cation 2 has the larger atom numbers. Image generated using Mercury (Macrae *et al.*, 2020).

displacement decreases to 1.343 Å (Figure 7), and (as expected) the greatest differences are in the chiral piperidine rings. For the DFT-optimized cations, the displacement is 1.430 Å (Figure 8), and decreases only slightly to 1.370 Å under the inversion option (Figure 9). The conformational differences are, thus, in the direction expected from a change in

chirality, even though the chirality of the two molecules is the same.

The remaining discussion concentrates on the DFT-optimized structure. The best view of the crystal structure is down the *b*-axis (Figure 10). The crystal structure consists of alternating layers (parallel to the *ab*-plane) of planar

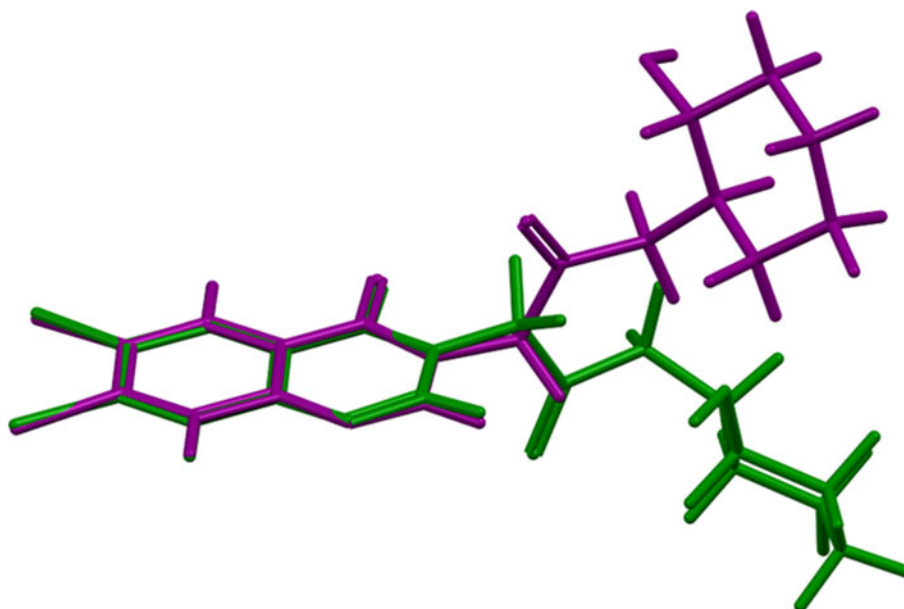
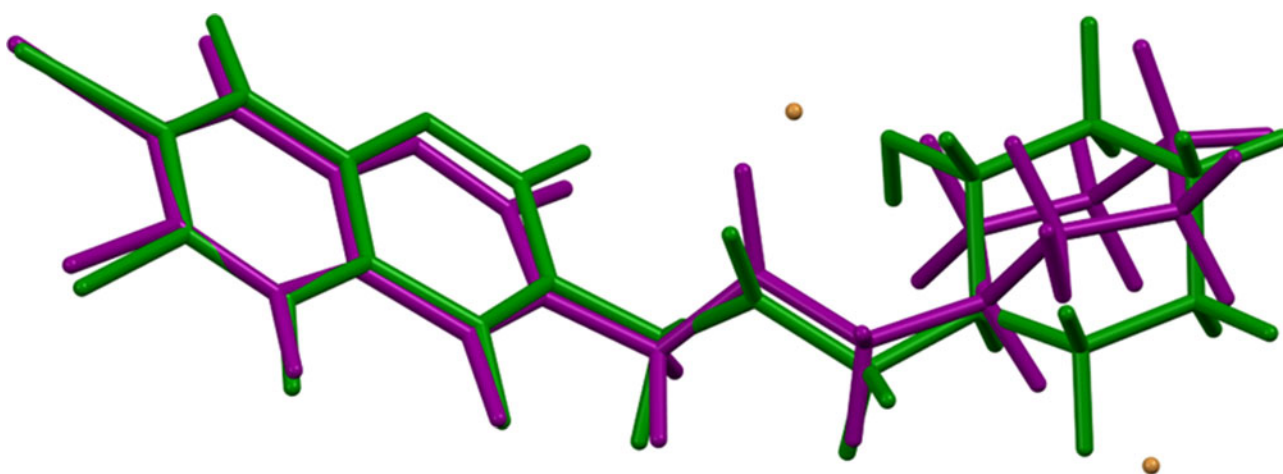


Figure 6. Comparison of cation 1 (purple) and cation 2 (green) in the refined structure of halofuginone hydrobromide, with the atoms of the quinazoline ring system superimposed (Mercury structure overlay). The rms Cartesian displacement of the ring atoms is 0.074 Å, while that of the whole molecules is 1.773 Å. Image generated using Mercury (Macrae *et al.*, 2020).

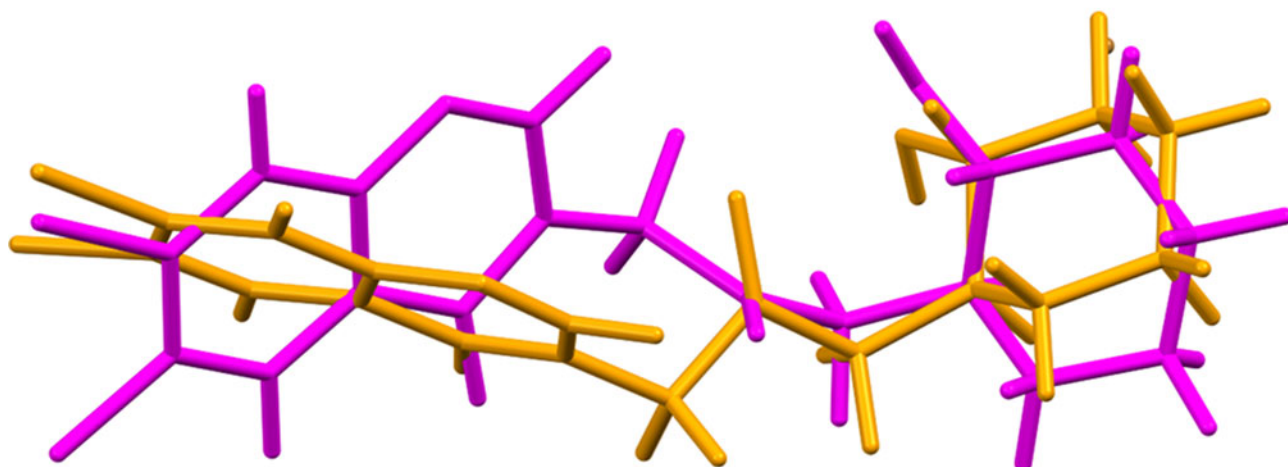


Invert; rmsd = 1.343

Figure 7. Comparison of cation 1 (purple) and cation 2 (green) in the refined structure of halofuginone hydrobromide, after the inversion option is invoked in Mercury. The rms Cartesian displacement is 1.343 Å. Image generated using Mercury (Macrae *et al.*, 2020).

and nonplanar portions of the cations. The average planes of the quinazoline ring systems are similar, at (7–18) for cation 1 and (4–14) for cation 2. The principal hydrogen bonds occur in the layers (parallel to the *ab*-plane) of piperidine rings.

All of the bond distances and bond angles fall within the normal ranges indicated by a Mercury/Mogul Geometry check (Macrae *et al.*, 2020). The torsion angles involving rotation about the C50–C55 bond in cation 2 are flagged as unusual. They lie on the tail of a gauche part of a bimodal distribution



DFT; mol 1 = orange, mol 2 = magenta; rmsd = 1.430

Figure 8. Comparison of cation 1 (orange) and cation 2 (magenta) in the VASP-optimized structure of halofuginone hydrobromide. The rms Cartesian displacement is 1.430 Å. Image generated using Mercury (Macrae *et al.*, 2020).

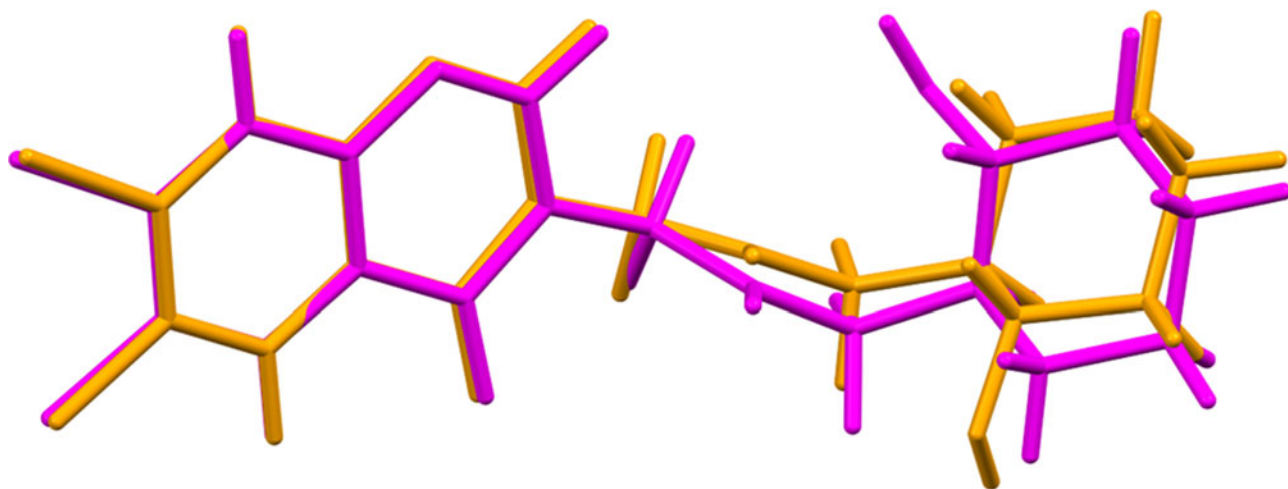
of similar torsion angles. These torsion angles, which indicate the angle of the piperidine ring with respect to the rest of the cation, seem to be slightly unusual.

Quantum chemical geometry optimization of the halofuginone cations (DFT/B3LYP/6-31G*/water) using Spartan '18 (Wavefunction, 2020) indicated that the observed conformation of cation 1 is 8.6 kcal mol⁻¹ higher in energy than the local minimum, and cation 2 is 8.5 kcal mol⁻¹ higher in energy. The local minimum of cation 1 is 0.5 kcal mol⁻¹ lower in energy than cation 2, within the expected error limits of such calculations, so the conformations should be considered equivalent in energy. The conformational differences are spread throughout the cations. Cation 1 is essentially in the global minimum-energy conformation. The different (but similar in energy) conformation of cation 2 shows that the cation is fairly flexible, and that intermolecular interactions are important in determining the solid-state conformations.

Analysis of the contributions to the total crystal energy of the structure using the Forcite module of Materials Studio (Dassault, 2021) suggests that the intramolecular deformation energy terms are small, but that angle deformation terms are the largest. The force-field-optimized structure reproduces the VASP-optimized structure (rms Cartesian displacements = 0.251 and 0.333 Å) better than the experimental structure (0.639 and 0.255 Å), but is closer to the experimental structure for cation 2. The intermolecular energy is dominated by electrostatic attractions, which in this force field analysis include hydrogen bonds. The hydrogen bonds are better analyzed using the results of the DFT calculation.

Hydrogen bonds are prominent in the structure (Table I). As expected, there are N–H...Br hydrogen bonds between the protonated piperidine nitrogen atoms H6 and H47 and the bromide anions Br83 and Br84, but only three of the four hydrogen atoms form such H-bonds. The remaining H33 forms a strong N–H...O hydrogen bond to the hydroxyl group O44. The energy of this N–H...O hydrogen bond is 6.6 kcal mol⁻¹, calculated using the correlation of Wheatley and Kaduk (2019). There are also O–H...Br hydrogen bonds between the hydroxyl groups O3 and O44 and the bromide anions. The N–H...Br and O–H...Br hydrogen bonds link the piperidine rings into a two-dimensional network parallel to the *ab*-plane. The methylene groups C16 and C57, and the aromatic carbon atoms C21 and C62, both form intramolecular C–H...O hydrogen bonds to the carbonyl groups O5 and O46. Cation 2 forms two additional C–H...O hydrogen bonds. The aromatic carbon atoms C22 and C63 form intermolecular C–H...N hydrogen bonds.

The Bravais–Friedel–Donnay–Harker (Bravais, 1866; Friedel, 1907; Donnay and Harker, 1937) morphology suggests that we might expect platy morphology for halofuginone hydrobromide, with {001} as the major faces. A fourth-order spherical harmonic preferred orientation model was included in the refinement. The texture index was 1.020(1), indicating that preferred orientation was minor for this rotated capillary specimen. The powder pattern of halofuginone hydrobromide from this synchrotron data set has been submitted to ICDD for inclusion in the Powder Diffraction File.



Invert; rmsd = 1.370

Figure 9. Comparison of cation 1 (orange) and cation 2 (magenta) in the VASP-optimized structure of halofuginone hydrobromide, after the inversion option is invoked in Mercury. The rms Cartesian displacement is 1.370 Å. Image generated using Mercury (Macrae *et al.*, 2020).

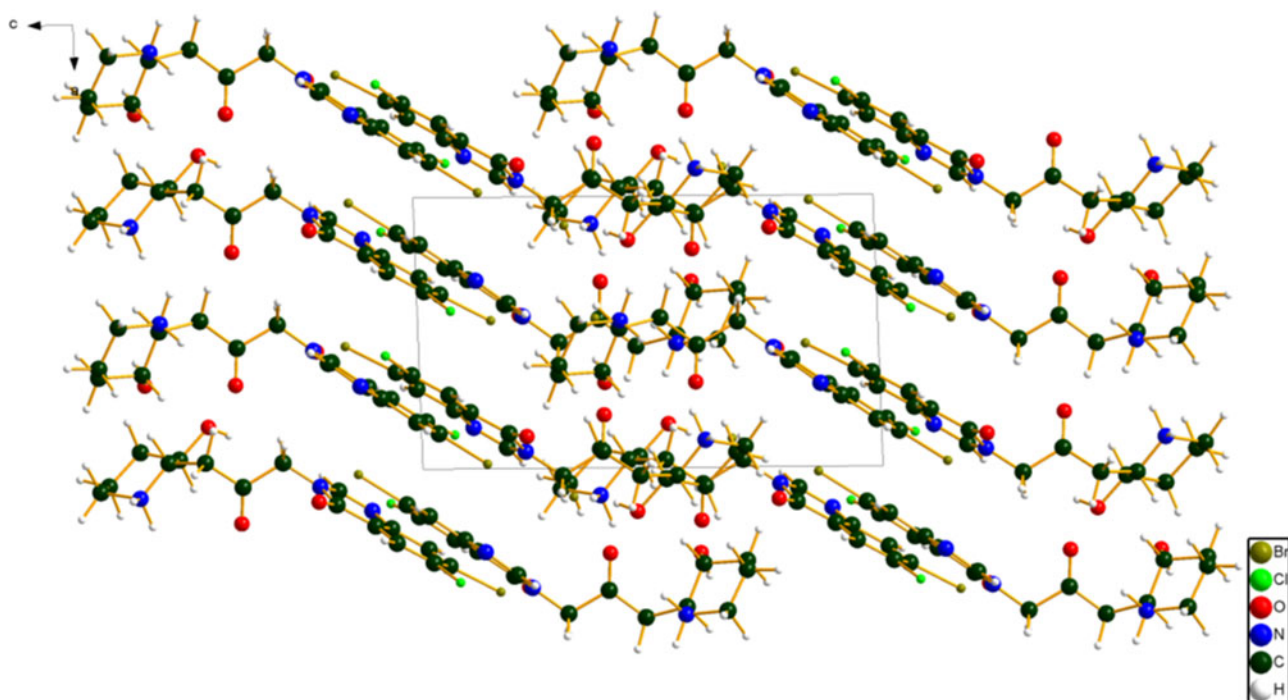


Figure 10. The crystal structure of halofuginone hydrobromide, viewed down the *b*-axis. Image generated using Diamond (Crystal Impact, 2022).

TABLE I. Hydrogen bonds (CRYSTAL17) in halofuginone hydrobromide

H-Bond	D-H (Å)	H...A (Å)	D...A (Å)	D-H...A (°)	Overlap (e)
N6-H33...O44	1.052	1.794	2.791	156.6	0.081
N6-H85...Br84	1.052	2.286	3.239	150.0	0.041
N47-H74...Br83	1.058	2.181	3.233	172.4	0.052
N47-H86...Br84	1.052	2.297	3.257	150.9	0.036
O3-H36...Br84	0.991	2.233	3.179	159.1	0.025
O44-H77...Br83	1.006	2.070	3.066	170.4	0.033
C19-H39...Br84	1.096	2.756	3.764	152.7	0.009
C60-H80...Br83	1.097	2.975	4.067	173.8	0.010
C16-H37...O5	1.101	2.328 ^a	2.739	99.8	0.018
C57-H78...O46	1.101	2.428 ^a	2.716	92.9	0.012
C21-H40...O5	1.091	2.587 ^a	2.881	94.3	0.012
C62-H81...O46	1.090	2.600 ^a	2.890	94.1	0.012
C12-H29...O45	1.101	2.310	3.313	150.5	0.016
C53-H71...O4	1.101	2.468	3.482	152.4	0.012
C50-H66-O3	1.101	2.051	3.043	148.4	0.040
C53-H70...O46	1.097	2.334	3.164	131.0	0.015
C22-H41...N49	1.092	2.558	3.586	156.5	0.021
C63-H82...N8	1.092	2.406	3.477	166.6	0.026

^aIntramolecular.

IV. DEPOSITED DATA

The Crystallographic Information Framework (CIF) files containing the results of the Rietveld refinement (including the raw data) and the DFT geometry optimization were deposited with the ICDD. The data can be requested at pdj@icdd.com.

ACKNOWLEDGEMENTS

The use of the Advanced Photon Source at Argonne National Laboratory was supported by the U.S. Department of Energy, Office of Science, Office of Basic Energy Sciences, under Contract No. DE-AC02-06CH11357. This work was partially supported by the International Centre for Diffraction Data. We thank Lynn Ribaud and Saul Lapidus for their assistance in the data collection.

CONFLICT OF INTEREST

The authors have no conflicts of interest to declare.

- Altomare, A., C. Cuocci, C. Giacovazzo, A. Moliterni, R. Rizzi, N. Corriero, and A. Falcicchio. 2013. "EXPO2013: A Kit of Tools for Phasing Crystal Structures from Powder Data." *Journal of Applied Crystallography* 46:1231–35.
- Antao, S. M., I. Hassan, J. Wang, P. L. Lee, and B. H. Toby. 2008. "State-of-the-art High-Resolution Powder X-ray Diffraction (HRPXRD) Illustrated with Rietveld Refinement of Quartz, Sodalite, Tremolite, and Meionite." *Canadian Mineralogist* 46:1501–9.
- Bravais, A. 1866. *Etudes Cristallographiques*. Paris: Gauthier Villars.
- Bruno, I. J., J. C. Cole, M. Kessler, J. Luo, W. D. S. Motherwell, L. H. Purkis, B. R. Smith, R. Taylor, R. I. Cooper, S. E. Harris, and A. G. Orpen. 2004. "Retrieval of Crystallographically-Derived Molecular Geometry Information." *Journal for Chemical Information and Computer Scientists* 44:2133–44.
- Crystal Impact - Dr. H. Putz & Dr. K. Brandenburg. 2022. *Diamond - Crystal and Molecular Structure Visualization*. Bonn, Germany. <https://www.crystalimpact.de/diamond>.
- Dassault Systèmes. 2021. *Materials Studio 2021*. San Diego CA: BIOVIA.

- Donnay, J. D. H., and D. Harker. 1937. "A New Law of Crystal Morphology Extending the Law of Bravais." *American Mineralogist* 22:446–7.
- Dovesi, R., A. Erba, R. Orlando, C. M. Zicovich-Wilson, B. Civalleri, L. Maschio, M. Rerat, S. Casassa, J. Baima, J. Salustro, and B. Kirtman. 2018. "Quantum-Mechanical Condensed Matter Simulations with CRYSTAL." *WIREs Computational Molecular Science* 8:e1360.
- Friedel, G. 1907. "Etudes sur la loi de Bravais." *Bulletin de la Société française de Minéralogie* 30:326–455.
- Gates-Rector, S., and T. Blanton. 2019. "The Powder Diffraction File: A Quality Materials Characterization Database." *Powder Diffraction* 39 (4):352–60.
- Gatti, C., V. R. Saunders, and C. Roetti. 1994. "Crystal-Field Effects on the Topological Properties of the Electron-Density in Molecular Crystals - the Case of Urea." *Journal of Chemical Physics* 101:10686–96.
- Groom, C. R., I. J. Bruno, M. P. Lightfoot, and S. C. Ward. 2016. "The Cambridge Structural Database." *Acta Crystallographica Section B: Structural Science, Crystal Engineering and Materials* 72:171–9.
- Kaduk, J. A., C. E. Crowder, K. Zhong, T. G. Fawcett, and M. R. Suchomel. 2014. "Crystal Structure of Atomoxetine Hydrochloride (Strattera), C₁₇H₂₃NOCl." *Powder Diffraction* 29 (3):269–73.
- Kim, S., J. Chen, T. Cheng, A. Gindulyte, J. He, S. He, Q. Li, B. A. Shoemaker, P. A. Thiessen, B. Yu, L. Zaslavsky, J. Zhang, and E. E. Bolton. 2019. "PubChem 2019 Update: Improved Access to Chemical Data." *Nucleic Acids Research* 47 (D1):D1102–9. doi:10.1093/nar/gky1033.
- Kresse, G., and J. Furthmüller. 1996. "Efficiency of Ab-Initio Total Energy Calculations for Metals and Semiconductors Using a Plane-Wave Basis Set." *Computational Materials Science* 6:15–50.
- Lee, P. L., D. Shu, M. Ramanathan, C. Preissner, J. Wang, M. A. Beno, R. B. Von Dreele, L. Ribaud, C. Kurtz, S. M. Antao, X. Jiao, and B. H. Toby. 2008. "A Twelve-Analyzer Detector System for High-Resolution Powder Diffraction." *Journal of Synchrotron Radiation* 15 (5):427–32.
- Louër, D. and A. Boulton. 2014. "Some further Considerations in Powder Diffraction Pattern Indexing with the Dichotomy Method." *Powder Diffraction* 29:57–2.
- Macrae, C. F., I. Sovago, S. J. Cottrell, P. T. A. Galek, P. McCabe, E. Pidcock, M. Platings, G. P. Shields, J. S. Stevens, M. Towler, and P. A. Wood. 2020. "Mercury 4.0: From Visualization to Design and Prediction." *Journal of Applied Crystallography* 53:226–35.
- Materials Design. 2016. *MedeA 2.20.4*. Angel Fire, NM: Materials Design Inc.
- Peintinger, M. F., D. Vilela Oliveira, and T. Bredow. 2013. "Consistent Gaussian Basis Sets of Triple-Zeta Valence with Polarization quality for Solid-State Calculations." *Journal of Computational Chemistry* 34:451–9.
- Spek, A. L. 2009. "Structure Validation in Chemical Crystallography." *Acta Crystallographica Section D* 65:148–55.
- Sykes, R. A., P. McCabe, F. H. Allen, G. M. Battle, I. J. Bruno, and P. A. Wood. 2011. "New Software for Statistical Analysis of Cambridge Structural Database Data." *Journal of Applied Crystallography* 44:882–6.
- The European Agency for the Evaluation of Medicinal Products, Committee for Veterinary Medicinal Products. 2000. Halofuginone Summary Report, EMEA/MRL/741/00-FINAL.
- Toby, B. H., and R. B. Von Dreele. 2013. "GSAS II: The Genesis of a Modern Open Source all Purpose Crystallography Software Package." *Journal of Applied Crystallography* 46:544–9.
- van de Streek, J., and M. A. Neumann. 2014. "Validation of Molecular Crystal Structures from Powder Diffraction Data with Dispersion-Corrected Density Functional Theory (DFT-D)." *Acta Crystallographica Section B: Structural Science, Crystal Engineering and Materials* 70 (6):1020–32.
- Wang, J., B. H. Toby, P. L. Lee, L. Ribaud, S. M. Antao, C. Kurtz, M. Ramanathan, R. B. Von Dreele, and M. A. Beno. 2008. "A Dedicated Powder Diffraction Beamline at the Advanced Photon Source: Commissioning and Early Operational Results." *Review of Scientific Instruments* 79:085105.
- Wavefunction, Inc. 2020. *Spartan '18 Version 1.4.5*. Irvine, CA: Wavefunction Inc.
- Wheatley, A. M., and J. A. Kaduk. 2019. "Crystal Structures of Ammonium Citrates." *Powder Diffraction* 34:35–43.